

## PLANETARY LENSING SIGNALS OF HIGH-MAGNIFICATION EVENTS UNDER SEVERE FINITE-SOURCE EFFECT

CHEONGHO HAN AND DOEON KIM

Program of Brain Korea 21, Department of Physics,  
Chungbuk National University, Chongju 361-763, Korea; cheongho@astroph.chungbuk.ac.kr

*Submitted to The Astrophysical Journal*

### ABSTRACT

We investigate the effect of a finite source on the planetary-lensing signals of high-magnification events. From this, we find that the dependency of the finite-source effect on the caustic shape is weak and perturbations survive even when the source is substantially bigger than the caustic. Specifically, we find that perturbations with fractional magnification excess  $\geq 5\%$  survive when the source star is roughly 4 times bigger than the caustic. We also find characteristic features that commonly appear in the perturbation patterns of planetary lens systems affected by severe finite-source effect and thus can be used for the diagnosis of the existence of a companion. These features form in and around a circle with its center located at the caustic center and a radius corresponding to that of the source star. The light curve of an event where the source crosses these features will exhibit a distinctive signal that is characterized by short-duration perturbations of either positive or negative excess and a flat residual region between these short-duration perturbations.

*Subject headings:* gravitational lensing – planetary systems

### 1. INTRODUCTION

Since the first discovery in 2004, eight planets have been detected by using the microlensing method (Bond et al. 2004; Udalski et al. 2005; Beaulieu et al. 2006; Gould et al. 2006; Gaudi et al. 2008; Bennett et al. 2008; Dong et al. 2008). The microlensing method is important in various aspects of exoplanet studies. First, due to its high sensitivity to planets located in the outer region of planetary systems beyond the snow line, the microlensing method is complementary to other methods such as the radial velocity and the transit methods that are sensitive to planets orbiting close to their host stars. In addition, the sensitivity of the microlensing method extends to very low-mass planets and Earth-mass planets can be detected from ground-based observations. Furthermore, it is the only proposed method that can detect free-floating planets (Bennett & Rhie 2002; Han 2006) that are thought to be kicked out from planetary systems. The detection rate of microlensing planets is rapidly increasing and at least five additional planet candidates were detected during the 2007 and 2008 observation seasons (A. Gould 2008, private communication).

The microlensing signal of a planet is a perturbation to a smooth standard light curve of a primary-induced lensing event occurring on a background star (Mao & Paczyński 1991; Gould & Loeb 1992). The duration of the perturbation is short: several hours for an Earth-mass planet and several days even for a gas-giant planet. Thus it is difficult to detect planetary signals from microlensing survey observations where stars are monitored on a roughly nightly basis. Currently, the observational frequency required for planet detections is achieved by employing an early-warning system and follow-up observations, where the early-warning system (OGLE: Udalski et al. 1994; MOA: Bond et al. 2001) enables to issue alerts of ongoing events by analyzing data from survey observations real time and follow-up observations (PLANET: Kubas et al. 2008; Micro-FUN: Dong et al. 2006) are focused on these alerted events. However, the limited number of telescopes available for follow-up observations restricts the number of events that can be followed up at any

given time and thus priority is given to events which will maximize the planet detection probability. Currently, the highest priority is given to high-magnification events (Bond et al. 2002; Yoo et al. 2004). These events have high intrinsic planet detection efficiency because the source trajectories always pass close to the perturbation region around the central caustic induced by the planet (Griest & Safizadeh 1998).

Despite the high chance of perturbation, however, it is often thought that detecting low-mass planets through the channel of high-magnification events would be difficult. This thought is based on the fact that the central caustic induced by a low-mass planet is usually smaller than the source star and thus the planetary signal would be greatly washed out by severe finite-source effect (Bennett & Rhie 1996). However, it might be that perturbations persist despite the finite-source effect and could still be detected thanks to the high photometry precision achieved by the enhanced brightness of the highly magnified source star. In this paper, we test this possibility by investigating how the pattern of central planetary perturbations is affected by the finite-source effect.

The paper is organized as follows. In § 2, we briefly describe the physical properties of central caustics. In § 3, we investigate the effect of a source size on the perturbation pattern. For this, we construct maps of perturbation pattern for planetary systems with various caustic/source size ratios and caustic shapes. Based on these maps, we search for characteristic features that may be used to identify the existence of planets. We summarize the results and conclude in § 4.

### 2. CENTRAL CAUSTIC

A planetary lens corresponds to the case of a binary lens with a very low-mass companion. One important characteristic of binary lensing that differentiates it from those of single lensing is the formation of caustics, which represent the positions on the source plane where the lensing magnification of a point source becomes infinite. Then, the light curve of a lensing event resulting from the source trajectory approaching or crossing the caustic can be dramatically different from the smooth and symmetric light curve of a single-lensing event.

The set of caustics form closed curves, each of which is composed of concave curves (fold caustic) that meet at points (cusps). For a planetary case, there exist two sets of caustics. A single ‘central caustic’ is located close to the primary lens and the other one or two ‘planetary caustics’ are located away from the primary.

Compared to size of the planetary caustic, the size of the central caustic is much smaller. When the size of the central caustic is measured as the separation between the two cusps located along the primary-planet axis, it is represented by (Chung et al. 2005)

$$\Delta\xi_{cc} \sim \frac{4q}{(s-s^{-1})^2} \propto q, \quad (1)$$

where  $q$  represents the planet/primary mass ratio and  $s$  is the primary-planet separation normalized by the Einstein radius corresponding to the total mass of the planetary system. On the other hand, the size of the planetary caustic is<sup>1</sup> (Han 2006)

$$\Delta\xi_{pc} \sim \frac{4q^{1/2}}{s(s^2-1)^{1/2}} \propto q^{1/2}. \quad (2)$$

Then, the size ratio between the two types of caustic is

$$\frac{\Delta\xi_{cc}}{\Delta\xi_{pc}} = \frac{q^{1/2}}{(1-s^2)^{3/2}} \propto q^{1/2}. \quad (3)$$

Considering that the size ratio is proportional to  $q^{1/2}$  and the mass ratio is very small for planetary lenses, the central caustic is much smaller than the planetary caustic. In addition, the size ratio becomes even smaller for lower mass planets.

The small size of a central caustic implies that the planetary signal induced by the central caustic is more likely to be affected by larger finite-source effect. The finite-source effect smears out the planetary signal because the magnification of a finite source corresponds to the magnification averaged over the source-star surface, i.e.

$$A = \frac{\int_0^{\rho_*} I(r) A_p (|\mathbf{r} - \mathbf{r}_0|) r dr}{\int_0^{\rho_*} I(r) r dr}, \quad (4)$$

where  $\mathbf{r}_0$  is the displacement vector of the source center with respect to the lens,  $\mathbf{r}$  is the vector to a position on the source star surface from the center of the source star,  $I(r)$  represents the surface brightness profile of the source star,  $A_p$  is the point-source magnification, and  $\rho_*$  represents the source radius normalized by the Einstein radius.

While the size of the central caustic depends both on the mass ratio and the separation, the shape of the caustic is solely dependent on the separation. When the shape is quantified as the vertical/horizontal width ratio and the vertical width  $\Delta\eta_{cc}$  is measured as the separation between the two off-axis cusps, the width ratio is related to the planetary separation by (Chung et al. 2005)

$$\frac{\Delta\eta_{cc}}{\Delta\xi_{cc}} = \frac{(s-s^{-1})^2 |\sin^3 \phi|}{(s+s^{-1}-2\cos\phi)^2}, \quad (5)$$

where

$$\phi = \cos^{-1} \left\{ \frac{3}{4}(s+s^{-1}) \left[ 1 - \sqrt{1 - \frac{32}{9}(s+s^{-1})^{-2}} \right] \right\}. \quad (6)$$

<sup>1</sup> We note that the expression in eq. (2) is for caustics of planetary lenses with  $s > 1$ . The planetary caustic for the case of  $s < 1$  has a different dependency on  $s$ , but it has the same dependency on  $q$ , i.e.  $\propto q^{1/2}$  (Han 2006).

For a given mass ratio, a pair of central caustics with separations  $s$  and  $s^{-1}$  are identical to the first order of approximation.

### 3. PERTURBATION PATTERN

The pattern of planetary perturbation is determined by two major factors. The first factor is the caustic shape and it determines the basic pattern of the perturbation. The second factor is the size ratio between the caustic and the source star and it characterizes how the pattern is deformed by the finite-source effect.

To see how a source size affects the pattern of central perturbations, we construct maps of *magnification excess* in the region around central caustics with various shapes and sizes. The magnification excess is defined by

$$\epsilon = \frac{A - A_0}{A_0}, \quad (7)$$

where  $A$  and  $A_0$  represent the lensing magnifications with and without the planet, respectively.

Figure 1 show the constructed maps. In the figure, the panels in each column show the pattern variation depending on the caustic shape, while the panels in each row show the variation depending on the caustic/source size ratio. We note that all caustics have an identical size as measured by the horizontal width  $\Delta\xi_{cc}$ . In each map, the regions with brown and blue-tone colors represent the areas where the planetary-lensing magnification is higher ( $\epsilon > 0$ ) and lower ( $\epsilon < 0$ ) than the single-lensing magnification, respectively. For each tone, the color changes into dark scales when the excess is  $|\epsilon| \geq 2\%$ , 3%, 5%, and 7%, respectively. The coordinates  $(\xi, \eta)$  are aligned so that  $\xi$  axis matches the primary-planet axis and the center is located at the effective position of the primary lens. The effective lens position represents the location of a single lens around which the magnification best describes that of the planetary lensing and it approximately corresponds to the center of the caustic. For a planetary case, the effective position has an offset from the original position of the primary of

$$\delta = \begin{cases} s^{-1}q/(1+q) & \text{for } s > 1, \\ -s[(1+q)^{-1}-1] & \text{for } s < 1, \end{cases} \quad (8)$$

where the sign is positive when the offset vector is directed toward the planet. In the map, the planet is located on the right and all lengths are normalized by the Einstein radius. We take the finite-source effect into consideration by modelling the source brightness profile as

$$\frac{I(\theta)}{I_0} = 1 - \Gamma \left( 1 - \frac{3}{2} \cos \theta \right) - \Lambda \left( 1 - \frac{5}{4} \cos^{1/2} \theta \right), \quad (9)$$

where  $\theta$  is the angle between the normal direction to the source-star surface and the line of sight. We adopt a linear and a square-root limb-darkening coefficients of  $(\Gamma, \Lambda) = (-0.46, 1.11)$ . The relation between the source and caustic sizes is marked on the top of each column. The primary-planet separation and the planet/primary mass ratio of the planetary system are marked on the right side of each row.

Considering that the caustic shape is characterized solely by the primary-planet separation and for a fixed planet/primary mass ratio the caustic size is linearly proportional to the mass ratio, one can picture excess maps for other cases of planetary systems based on the presented maps in Figure 1. For example, a planetary system with  $(s, q) = (2.0, 1.67 \times 10^{-4})$  has a similar perturbation pattern to that of the system with

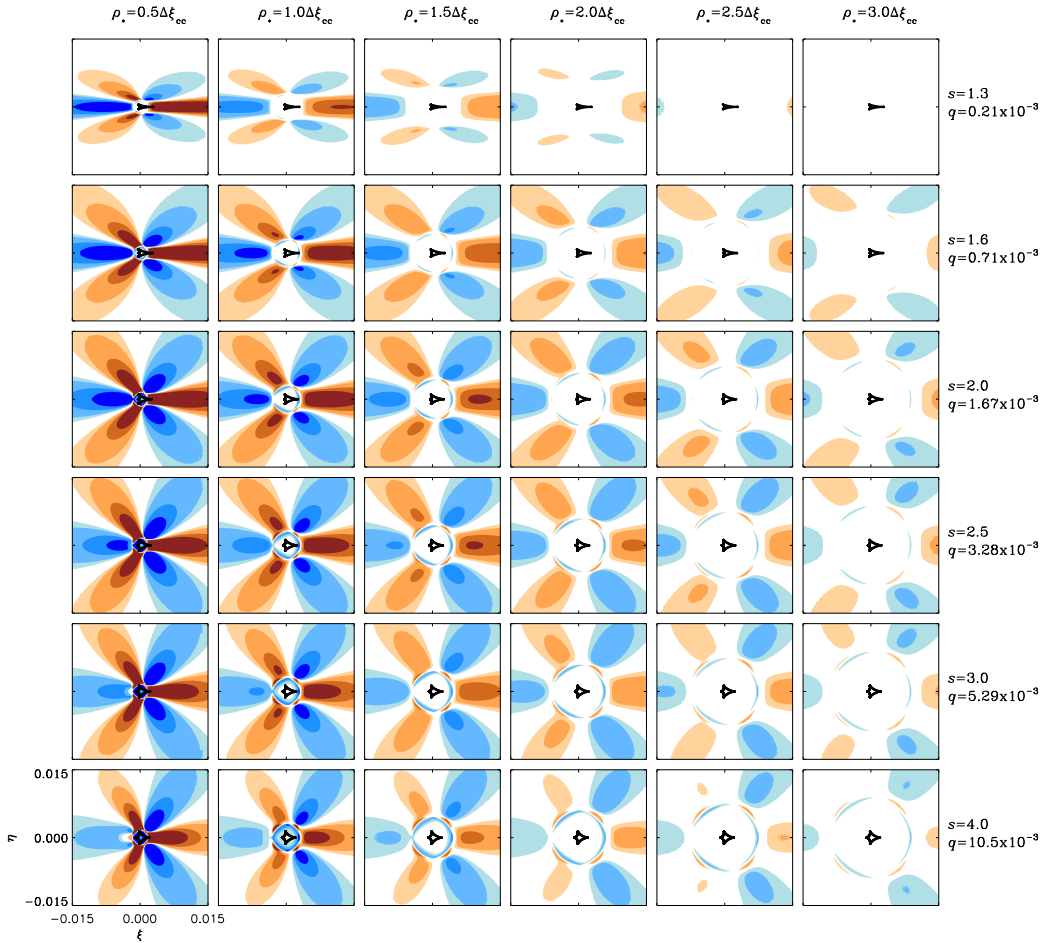


FIG. 1.— Maps of magnification excess around the region of central caustics with various shapes and caustic/source size ratios. In the figure, the panels in each column show the pattern variation depending on the caustic shape, while the panels in each row shows the variation depending on the caustic/source size ratio. In each map, the regions with brown and blue-tone colors represent the areas where the planetary lensing magnification is higher ( $\epsilon > 0$ ) and lower ( $\epsilon < 0$ ) than the single-lensing magnification, respectively. For each tone, the color changes into dark scales when the excess is  $|\epsilon| \geq 2\%$ ,  $3\%$ ,  $5\%$ , and  $7\%$ , respectively. The coordinates  $(\xi, \eta)$  are aligned so that  $\xi$  axis matches the star-planet axis and the center is located at the effective position of the primary lens around which the single-lensing magnification best describes that of the planetary lensing. The planet is located on the right. All lengths are in units of the Einstein radius corresponding to the total mass of the lens system. The relation between the source and caustic sizes is marked on the top of each column. The primary-planet separation and the mass ratio are marked on the right side of each row.

$(s, q) = (2.0, 1.67 \times 10^{-3})$ . The only major difference is that the scale of the map decreases by a factor 10 because the caustic becomes smaller. We also note that the perturbation patterns of a pair of planetary systems with  $s$  and  $s^{-1}$  are identical and thus one can infer perturbation patterns for the cases of planetary systems with  $s < 1$  from those presented in the figure.

From the analysis of the maps, we find that the dependency of the finite-source effect on the caustic shape is weak and perturbations persist even when the source is substantially bigger than the caustic. Specifically, we find that perturbations with  $\epsilon \geq 5\%$  survive when the source star (as measured by its diameter) is roughly 4 times bigger than the caustic, i.e.  $\rho_* \sim 2\Delta\xi_{cc}$ . Based on this, Han (2008) derived an analytic expression for the optimal range of planetary separations (lensing zone) detectable through the channel of high-magnification events of

$$\left| \sqrt{\frac{2q}{\rho_*}} - \sqrt{\frac{2q}{\rho_*} + 1} \right| \lesssim s \lesssim \sqrt{\frac{2q}{\rho_*}} + \sqrt{\frac{2q}{\rho_*} + 1}. \quad (10)$$

Then, the lensing zone of central perturbations (central lens-

ing zone) is different for planets with different mass ratios unlike the fixed range of the classical lensing zone ( $0.6 \lesssim s \lesssim 1.6$ ) regardless of the mass ratio (Wambsganss 1997; Griest & Safizadeh 1998). According to this expression, the central lensing zone is larger than the classical lensing zone for planets with  $q \gtrsim 3 \times 10^{-4}$  despite the smaller size of the central caustic than the size of the planetary caustic.

From the maps, we also find interesting features in the region near the boundary and inside of a circle with its center located at the caustic center and a radius corresponding to that of a source star. These features are the localized arc-shaped perturbation regions with either positive or negative excess located at the edge of the circle and the region inside the circle with a very small magnification excess. We find that these features commonly appear in the perturbation patterns affected by severe finite-source effect.

For close investigation of these features, we construct a separate set of excess maps of a planetary lens with and without the finite-source effect. These maps are presented in Figure 2. In the map, all lengths are scaled by the source radius to better show the location of the features in units of the source radius.

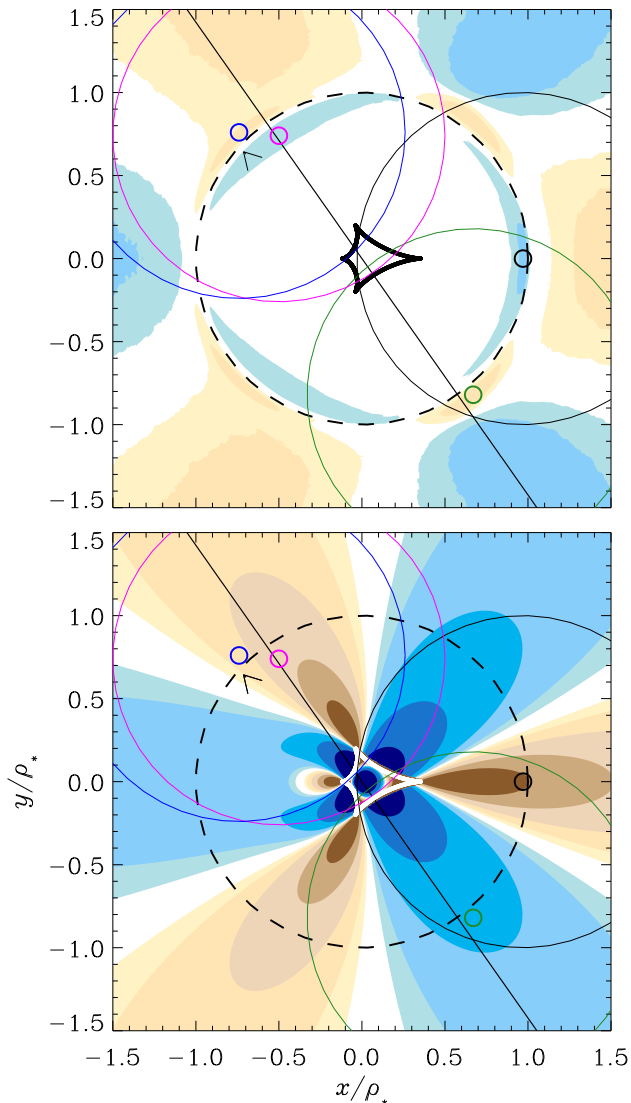


FIG. 2.— Excess maps of a planetary lens with (upper panel) and without (lower panel) finite-source effect. Notations are similar to those of Fig. 1 except two things. The first difference is that all lengths are scaled by the source radius not by the Einstein radius. Another difference is that the color scale changes at the levels of  $|\epsilon| = 2\%$ ,  $4\%$ ,  $8\%$ ,  $16\%$ , and  $32\%$ , respectively. Five circles are drawn in each map. All circles have a common radius corresponding to the source radius. The center of the black dashed circle is located at the effective primary position. The centers of other circles are located at the mid-points of the individual arc-shaped perturbation regions. The planetary lens parameters are  $s = 0.38$  and  $q = 2.27 \times 10^{-3}$  and the source radius is  $\rho_* = 3.14 \times 10^{-3}$ .

Another difference of the maps from those presented in Figure 1 is that the color scale changes at the levels of  $|\epsilon| = 2\%$ ,  $4\%$ ,  $8\%$ ,  $16\%$ , and  $32\%$ , respectively, to emphasize the region of very high excesses. Five circles are drawn on each map. All circles have a common radius corresponding to the source radius. The center of the black dashed circle is located at the caustic center. The centers of other circles are located at the mid-points of the individual arc-shaped perturbation regions.

Close inspection of the pattern leads us to find the following tendencies. First, we find that the very small excess in the region inside the dashed circle is caused by the cancellation of the positive and negative excesses. When the center of the

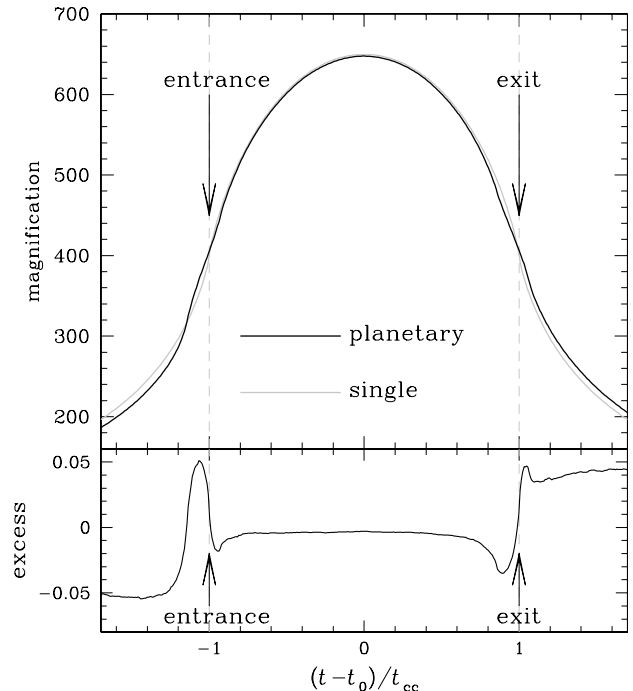


FIG. 3.— A characteristic planetary signal in the light curve of a high-magnification event affected by severe finite-source effect. The signal is characterized by short-duration perturbations of either positive or negative excess at the moments when the center of the central caustic enters into and exits from the source star and a flat residual between the short-duration perturbations.

source star is located within this area, the amount of positive and negative excesses balances each other, resulting in a very small excess. However, when the source center is located outside of this area, this balance breaks down and perturbation features show up.

Second, we find that the arc-shaped perturbation features are caused by the localized regions of very large excesses around the caustic. Such regions include the regions just outside the cusps with very large positive excesses and the regions just outside the fold caustics with very large negative excesses. Another region of a very large negative excess is the region inside the caustic. The localized arc-shaped perturbation regions form at the source position where the source star encompasses some of these strong perturbation regions and the resulting overall excess is seriously unbalanced. For example, when the source star is located at the position of the blue circle, it encompasses two large positive-excess regions around two cusps but only a single large negative-excess region between the cusps. As a result, the overall excess is positive. By contrast, when the source star is located at the adjacent position of the magenta circle, it encompasses the same number of the two large positive-excess regions but now four large negative-excess regions including two additional regions around fold caustics and one inside the caustic, resulting in an overall negative excess. The other perturbation regions can be explained in a similar way.

The existence of the characteristic features in the pattern of central perturbation region provides an important diagnostic tool that can be used to identify the existence of a companion for a high-magnification event affected by severe finite-source effect. This is because the light curve of an event where the source crosses these features will exhibit a distinctive signal

that is characterized by short-duration perturbations of either positive or negative excess and a flat residual region between these short-duration perturbations. We present an example light curve of such an event in Figure 3. Recently, a planetary-lensing event exhibiting a similar planetary signal was actually detected (MOA-2007-BLG-400: Dong et al. 2008). Considering that high-magnification events are prime targets of the current microlensing follow-up observations, we predict that more of such planetary signals would be detected.

We note, however, that the existence of these characteristic signals does not necessarily confirm the existence of a planetary companion. This is because such signals can also be produced by a wide ( $s \gg 1.0$ ) or a close ( $s \ll 1.0$ ) binary companions that can also give rise to small central caustics. Therefore, detailed modeling should be done for the complete characterization of the lens system.

#### 4. SUMMARY AND CONCLUSION

We investigated the effect of a finite source on the central perturbation pattern. From this, we found that the dependency of the finite-source effect on the caustic shape is weak and

perturbations survive even when the source is substantially bigger than the caustic. Specifically, we found that perturbations with fractional magnification excess  $\geq 5\%$  survive when the source star is roughly 4 times bigger than the caustic. We also found characteristic features that commonly appear in the perturbation patterns of lens systems affected by severe finite-source effect and thus can be used for the diagnosis of the existence of a companion. These features form in and around a circle with its center located at the caustic center and a radius corresponding to that of the source star. The light curve of an event where the source crosses these features will exhibit a distinctive signal that is characterized by short-duration perturbations of either positive or negative excess and a flat residual region between these short-duration perturbations.

This work was supported by the Astrophysical Research Center for the Structure and Evolution of the Cosmos (ARC-SEC) of Korea Science and Engineering Foundation (KOSEF) through Science Research Center (SRC) program.

#### REFERENCES

- Beaulieu, J. P., et al. 2006, *Nature*, 439, 437  
 Bennett, D. P., & Rhie, S. H. 1996, *ApJ*, 472, 660  
 Bennett, D. P., & Rhie, S. H. 2002, *ApJ*, 574, 985  
 Bennett, D. P., et al. 2008, *ApJ*, 684, 663  
 Bond, I. A., et al. 2001, *MNRAS*, 327, 868  
 Bond, I. A., et al. 2002, *MNRAS*, 333, 71  
 Bond, I. A., et al. 2004, *ApJ*, 606, L155  
 Chung, S.-J., et al. 2005, *ApJ*, 630, 535  
 Dong, S., et al. 2006, *ApJ*, 642, 842  
 Dong, S., et al. 2008, *ApJ*, submitted  
 Gaudi, B. S., et al. 2008, *Science*, 319, 927  
 Gould, A., et al. 2006, *ApJ*, 644, L37  
 Gould, A., & Loeb, A. 1992, *ApJ*, 396, 104  
 Griest, K., & Safizadeh, N. 1998, *ApJ*, 500, 37  
 Han, C. 2006, *ApJ*, 638, 1080  
 Han, C. 2006, *ApJ*, 644, 1232  
 Han, C. 2008, *ApJ*, submitted  
 Kubas, D., et al. 2008, *A&A*, 483, 317  
 Mao, S., & Paczyński, B. 1991, *ApJ*, 374, L37  
 Udalski, A., et al. 2005, *ApJ*, 628, L109  
 Udalski, A., Szymański, M., Kałużny, J., Kubiak, M., Mateo, M., Krzemiński, W., & Paczyński, B. 1994, *Acta Astron.*, 44, 227  
 Wambsganss, J. 1997, *MNRAS*, 284, 172  
 Yoo, J., et al. 2004, *ApJ*, 616, 1204